Harnessing laser technology to create stable metal halide perovskite–rGO conjugates as promising electrodes for Zn-ion capacitors†

Athanasia Kostopoulou, [iD] *[a] Dimitra Vernardou,*[b] Nikolaos Livakas,[a] Konstantinos Brintakis, [iD] [a] Stylianos Daskalakis [iD] [b] and Emmanuel Stratakis [iD] *[a,c]

We report that the direct conjugation of metal halide perovskite nanocrystals on rGO sheets can provide high performance and stable electrodes for Zn-ion capacitors. It is the first time that metal halide nanocrystals have been used to enhance the energy storage of 2D materials in capacitors by introducing an additional pseudocapacitance mechanism. In particular, we present a simple, rapid and room temperature laser-induced method to anchor $CsPbBr_3$ nanocrystals on rGO sheets without affecting the initial morphology and crystal structure of the two components. The flexible and high surface area of the rGO sheets enables the conjugation of individual metal halide perovskite nanocrystals, giving rise to new synergetic functionalities. As a result, the specific capacitance of the perovskite–rGO conjugated electrodes can be enhanced by 178- and 152-times compared to those of the plain rGO and perovskite electrodes respectively.

1. Introduction

To meet the world's energy needs, simultaneous development of energy conversion and energy storage systems is required. At the same time, the investigation of efficient energy-assisted, low-cost, fast and solution-processable new materials for these energy-related applications is essential.[1,2] Metal halide perovskites play a prominent role as active materials in photovoltaic solar cells, leading to high performance, competitive with those of well-established technologies.[1,2] Nevertheless, the study of metal halide perovskite materials in energy storage devices is still limited and mainly focused on batteries. Hybrid

[a]*Institute of Electronic Structure and Laser, Foundation for Research and Technology - Hellas, Heraklion, 71110 Crete, Greece. E-mail: akosto@iesl.forth.gr, stratak@iesl.forth.gr*
[b]*Department of Electrical & Computer Engineering, School of Engineering, Hellenic Mediterranean University, Heraklion, 710 04 Crete, Greece. E-mail: dvernardou@hmu.gr*
[c]*Department of Physics, University of Crete, 71003 Heraklion, Greece*
†Electronic supplementary information (ESI) available. See DOI: https://doi.org/10.1039/d3nr05552c

organic–inorganic and all-inorganic metal halide perovskite materials in nanocrystal,[3,4] microcrystal[5–10] or film-like structures[11] have been proposed as anode materials in Li-based batteries with the highest specific discharge capacity of 549 mA h g^{-1} with an optimum stability of 1500 cycles.[7] On the other hand, the utilization of metal halide perovskites in capacitors as electrode elements due to their high ionic conductivity[12–18] leads to a maximum capacitance of 3.32 F cm^{-2} for a Pb-free hybrid bismuth-halide complex $(CN_2SH_5)_3BiI_6$,[14] while an enhanced value of 121 F g^{-1} was achieved for all-inorganic $CsPbBr_3$ reported by Thakur *et al.* two years later.[19]

In addition, 2D graphene-related materials have been introduced as great candidates for both batteries and capacitors due to their high electrical conductivity.[20] They are easily fabricated and relatively cheap with characteristic permeability, facilitating the efficient penetration of electrolytes into electrodes and boosting the capacitance of storage devices.[21] Their unique physicochemical features such as high morphological anisotropy, high specific surface area, different active sites, and tunable physicochemical properties, together with their flexibility and thermal/chemical stability, led the scientific community to use them as anodes in Li batteries with good capacity and cycling lifetime.[22] The maximum charge capacity of graphite in Li batteries was found to be up to 372 mA h g^{-1},[23] while the theoretical capacity of graphene reached a value of 744 mA h g^{-1}.[24] Graphene sheets can buffer the volume effect of anode materials during charge and discharge and improve their electronic conductivity, while graphene/metal (metal oxide) composites can be used as battery cathodes to improve their cycling performance.[20,24,25] In this context, the improvement of capacitor performance can be accomplished through the fabrication of hybrid two-component electrodes that couple transition metal oxides with graphene-based materials and take advantage of the synergy between the electric double layer capacitor (EDLC) and pseudocapacitance originating from the two components. Transition metal oxides, in particular, have been investigated as promising electrode materials for capacitors due to their

high capacitance obtained *via* quick and reversible redox processes at their surfaces, but they suffer from low conductivity.[26] Accordingly, a specific capacitance value of 389 F g^{-1} was achieved for the MnO_2–graphite hybrid composite,[27] which is superior to the MnO_2-rGO (135.5 F g^{-1})[28] and MnO_2-GO (197.2 F g^{-1})[29] composites. A significantly enhanced value has also been found in the case of silver-doped MnO_2 coupled with GO (877 F g^{-1})[30] and Cu oxide on amine-functionalized GO (3890 F g^{-1}).[31] Further examples of hybrid composite materials with high specific capacitance are Co_3O_4 with graphene (243 F g^{-1})[32] or rGO (291 F g^{-1}),[33] ZnO with rGO (308 F g^{-1}),[34] CeO_2 with graphite (191 F g^{-1}),[35] and Fe_3O_4 with rGO (480 F g^{-1}).[36] Notably, there is no report on the combination of metal halide perovskites with graphene-related materials for application in capacitors.

Very recently, a new type of capacitor, namely a Zn-ion capacitor, has attracted significant attention due to its high theoretical capacity, safety, environmentally friendly nature, cost effectiveness, and the use of abundant elements; the abundance of Zn is ~300 times higher compared to that of lithium.[37,38] In order to obtain high performance and long-life Zn-ion capacitors, new electrode materials have to be explored. 2D materials are among potential candidates,[38] due to their low thickness, which shortens the charge diffusion path during charge and discharge cycles. On top of that, their ability to endure high strains could enhance the lifetime and stability of the respective energy storage devices.[38] Nevertheless, the electrochemical behavior of graphene-related materials is complicated because it is correlated to the number of defects, functional groups and impurities.[39] Very recently, Xu *et al.* revealed that in Zn-ion hybrid capacitors, apart from the contribution of oxygen-containing groups, an extra contribution from the reversible adsorption/desorption of H$^+$ on the carbon atoms of rGO sheets takes place.[40] Despite the great research on two-component storage materials incorporating graphene-related elements, the use of such materials in Zn-ion capacitors is limited. Among the research challenges to be addressed in two-component electrodes are the volume expansion and self-aggregation of nanomaterials.[38] In particular, rGO has been conjugated with NbPO,[41] carbon nanotubes[42] or $Co_xNi_{2-x}P$[43] with the latter one presenting the highest specific capacitance of 356.6 F g^{-1}. However, there is currently no report on the combination of rGO or other 2D materials with metal halide perovskites to be applied as electrode materials in Zn-ion capacitors.

In this work, we present for the first time the application of room temperature synthesized metal halide perovskite–rGO conjugated materials as electrodes in Zn-ion capacitors. Such conjugation has been realized *via* a femtosecond laser-induced process, which enables fine tuning of the areal density of nanocrystals anchored onto the rGO sheets while keeping the nanocrystals' size, morphology and crystallinity unaffected. It is shown that rGO functions as a conductive channel for charge transfer and energy storage *via* surface adsorption and desorption (electric double layer storage mechanism), as well as a template to induce the growth of individual metal halide

perovskite nanocrystals, which are responsible for the additional pseudocapacitance recorded. One of the benefits of this photo-induced method is the uniformity of the anchored nanocrystals, which is superior to that obtained with wet chemistry methods.[44–46]

2. Results and discussion

Motivated by works on combination of different materials for enhancing the electrodes' storage properties in capacitors[47–52] as well as the unique electrochemical and thermal/strain release properties of 2D materials,[22,38] the photo-assisted conjugation of metal halide perovskite nanocrystals with rGO nanosheets has been investigated. This is the first time that such a method has been utilized for the fabrication of potential electrode materials for Zn-based capacitors.

Specifically, well-crystalline and homogeneous photoluminescence (PL)-active $CsPbBr_3$ nanocrystals with a size of around 11 nm were synthesized using a room temperature approach based on ligand-assisted re-precipitation with slight modifications of the protocol previously reported by Li *et al.*[53] (Fig. S1 and S2†). Prior to the conjugation with amine-functionalized rGO, the exfoliation of bulk-like sheets was necessary (Fig. S3†). The thickness of the liquid-phase exfoliated sheets was determined to be 2.3 ± 0.2 nm. The two materials, namely the purified nanocrystals (Fig. 1a) and the exfoliated rGO sheets (Fig. 1b), were dispersed in a common solvent (toluene) (Fig. 1c) and irradiated with a femtosecond laser of 1026 nm wavelength using the set-up illustrated in Fig. S4.† Previous work of our group revealed the successful conjugation of perovskite nanocrystals (~100 nm) and GO sheets upon irradiation with a femtosecond laser of 513 nm wavelength.[54] In this work, irradiation with few-femtosecond pulses of 1026 nm wavelength under mild intensity conditions was efficient enough for the homogeneous distribution of small-sized perovskite nanocrystals (~11 nm) on the rGO sheets. Notably, the tuning of the nanocrystals' density anchored onto the rGO sheets upon irradiation with different numbers of irradiation pulses has been demonstrated (Fig. 1d–h).

Anchoring of nanocrystals was initially achieved by simple mixing of the two different materials' dispersion in a common solvent, attributed to the presence of amine functional groups on the rGO sheets (Fig. 1c). Subsequently, the number density of the anchored nanocrystals can be progressively increased upon irradiation (Fig. 1d–g). This was also confirmed by the suppression of PL upon laser irradiation (Fig. 1i). At the same time, the morphology and crystal structure of the perovskite nanocrystals were not altered upon irradiation, at least for the number of pulses below 10^5 (Fig. 1 and Fig. S5†). For a higher number of pulses, aggregation of nanocrystals was observed (Fig. 1h). In addition, Raman spectra recorded before and after irradiation verified the non-alteration of the rGO component even after 60 million pulses (Fig. S6†).

The perovskite nanocrystal–rGO conjugates formed upon irradiation with 10^5 pulses were selected for their use as elec-
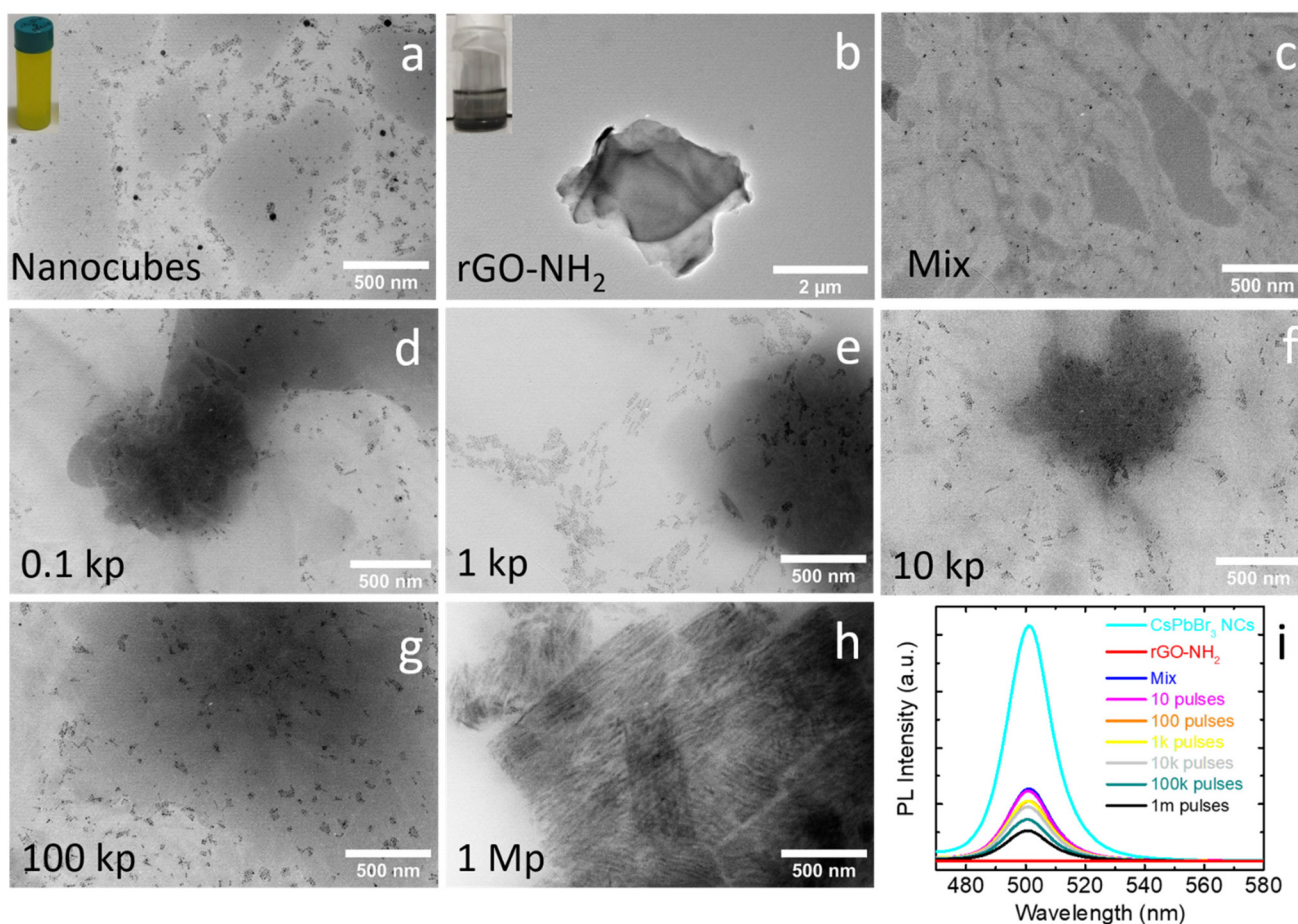
Fig. 1 Transmission electron microscopy (TEM) images of the metal halide perovskite nanocrystals (a), the amine-functionalized rGO sheets (b), a mixture of the two materials in toluene prior to irradiation (c), the conjugated dispersions after irradiation with 100−1 million pulses (d–h), and the corresponding PL curves (i). Insets in (a) and (b): digital photographs of the perovskite nanocrystals' and rGO sheets' toluene-based colloidal dispersions.

trodes in Zn-ion capacitors, due to the large number density and homogeneous distribution of individually anchored nano-crystals on the sheets (Fig. 1g). Specifically, the conjugates were deposited on a Ni substrate by drop-casting from the solution and subsequently covered by a thin layer of TiO_x deposited *via* pulsed laser deposition (PLD). As demonstrated in our previous works on Li–air batteries, the TiO_x layer contributes significantly to the improved stability of the perovskite-based electrodes.[3,7]

The cyclic voltammetry (CV) curves of the conjugate-based electrodes were examined at a scan rate of 100 mV s^{-1} for a potential range of −0.5 V to +1.0 V. A nearly quasi-rectangular curve was observed with a broad cathodic hump at approximately +0.65 V and an anodic hump at approximately +0.48 V, implying a pseudocapacitance behavior originating from the metal halide perovskite nanocrystals (Fig. 2a). In addition, a larger integral area and a two order higher magnitude of specific current were observed compared to the single-component electrodes (pure rGO or perovskite nanocrystals), suggesting a higher specific capacitance when the area of the

CV curve is proportional to the specific capacitance (Fig. 2b and c).

The excellent stability of the conjugation-based electrodes during the continuous Zn^{2+} intercalation/deintercalation scans was confirmed by the similarity of the CV shapes obtained from the first to the 100th scan (Fig. 2a). This behavior was in contrast to the single-perovskite nanocrystal electrodes that presented degradation from the very first cycling process (Fig. 2c).

To account for the mechanisms taking place during the Zn^{2+} intercalation/deintercalation within/from the conjugated materials, the CV characteristics were recorded at lower than 100 mV s^{-1} scan rates ranging from 4 to 10 mV s^{-1} (Fig. 2d). As was expected, the specific current was enhanced with an increase in the scan rate. Moreover, the peaks at ∼−0.36 V (cathodic/reduction) and ∼+0.56 V (anodic/oxidation) were shifted to more negative and positive values respectively, due to the electrochemical polarization effect.[55] Such an effect is attributed to the accumulation of charge on the electrode surface, which can result in a shift in the potential required
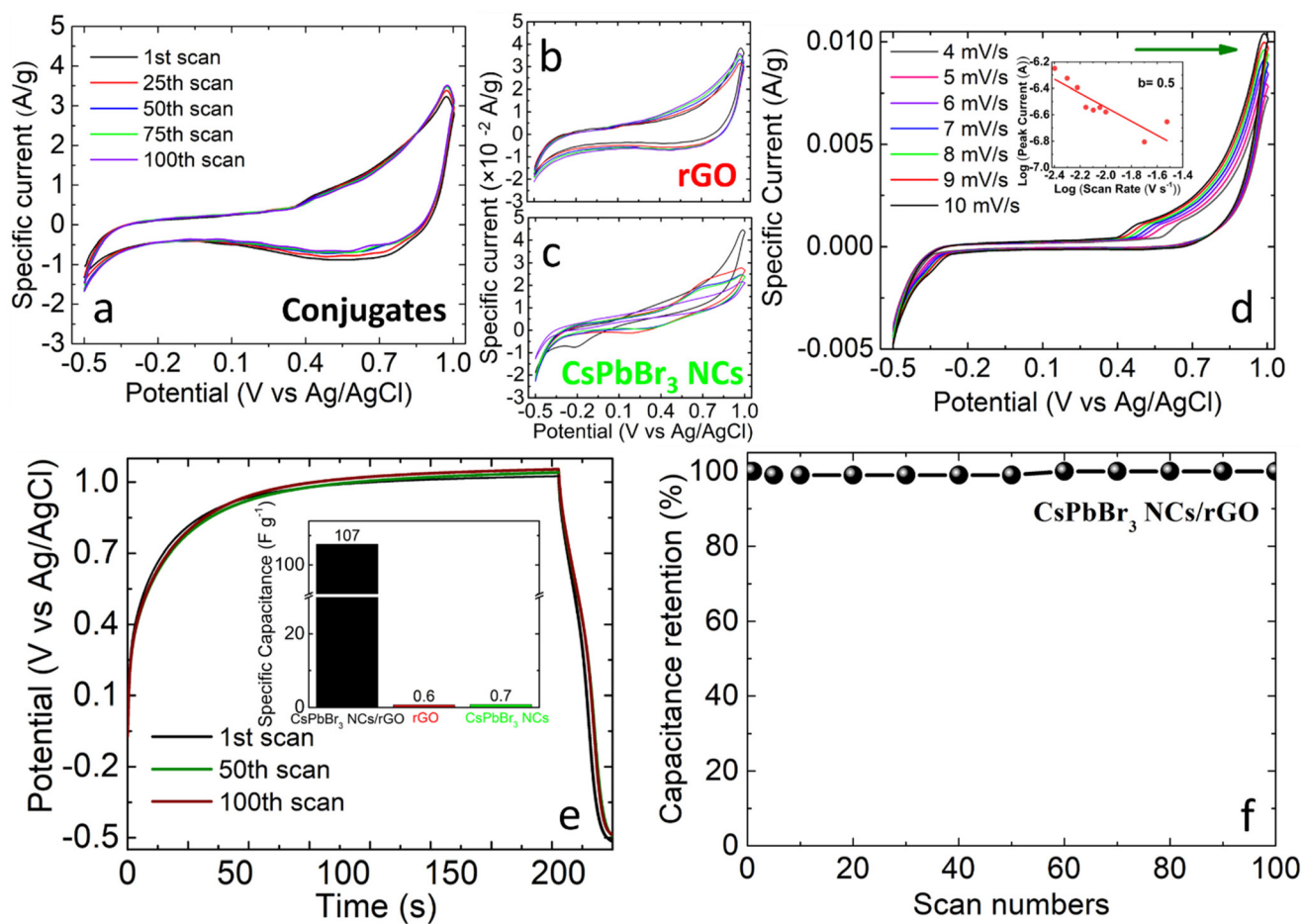
Fig. 2 Cyclic voltammograms of the anodes based on metal halide perovskite nanocrystal–rGO conjugates (a), pure rGO (b), and pure metal halide perovskite nanocrystals (c) that were traced at a constant scan rate of 100 mV s^{-1} and following a series of consecutive scans shown in the legends; cyclic voltammograms obtained at 4–10 mV s^{-1} (d). The inset shows the linear fitting used for the calculation of the b value; time dependence of the potential for the 1st, 50th and 100th scans at an applied specific current of 0.8 A g^{-1} (e). The inset shows a histogram plot comparing the specific capacitance between the conjugation-based electrodes (black column) and single-component electrodes (red and green columns for rGO and perovskite nanocrystals respectively); cyclic stability of the conjugation-based electrode (f).

for the oxidation (to more positive values) and reduction (to more negative values) processes. The relationship between the peak current, I, and the scan rate, v, obeys the equation $I = av^b$, where a and b are empirical constants. Specifically, the b value could be used to evaluate the energy storage mechanism; for b = 0.5, a diffusion-controlled process takes place, while for b = 1.0, a surface capacitive-controlled process occurs.[56,57] By linearly fitting $\log(I)$ as a function of $\log(v)$ in Fig. 2d, the b value was estimated to be 0.5 for the anodic peak (Fig. 2d inset), which implies a diffusion-controlled process. In contrast, upon increasing to a rate of 100 mV s^{-1} (Fig. 2a), such anodic/cathodic peaks were not detectable, indicating that the storage mechanism can be explained as an interplay between faradaic (pseudocapacitance) and non-faradaic processes. It is therefore a combination of Zn ion intercalation/deintercalation into the perovskite together with their adsorption on the rGO surface.

In addition, the characteristic curves obtained from galvanostatic measurements deviated from the typical triangular shape, providing additional evidence for the combination of the pseudocapacitance with the faradaic capacitance.[58] For the estimation of the specific capacitance, the equation $C_{sp} = (I \times t)/(\Delta V \times m)$ was used, where C_{sp} is the specific capacitance by mass of the active material, I is the applied current, t is the charge time and m is the mass of the active material.[59] It was found to be 107 F g^{-1} for the perovskite–rGO conjugates, 600 mF g^{-1} for pure NH$_2$-functionalized rGO and 700 mF g^{-1} for the pure perovskite electrodes (Fig. 2e inset). The enhancement of the specific capacitance observed in the case of the metal halide perovskite nanocrystals–rGO conjugated electrodes can be attributed to the fact that rGO serves as a conductive channel for charge transfer. As a result, it not only improves the overall conductivity of the electrode, but also acts as a flexible template to facilitate the growth of individual

metal halide perovskite nanocrystals that are responsible for the pseudocapacitance. It is important to mention that there is currently no report on the use of metal halide perovskite nanocrystals as pseudocapacitance elements for the enhancement of the specific capacitance of rGO electrodes in Zn-ion capacitors.

What is also observed is that the attainable potential difference value is higher for the perovskite–rGO electrodes, implying a more effective Zn^{2+} intercalation/deintercalation process compared to that occurred in the pure perovskite nanocrystal electrode (Fig. S7†). As a result, the conjugated structure enables a higher amount of charge storage and as a consequence a larger specific capacitance. Based on the time-dependence of the potential difference (Fig. S7†), a time constant can be calculated, defined as the time taken for V_c (potential difference across the electrodes) to achieve a maximum value of 63.2% denoted as V_s, which corresponds to the value of the supply. Indeed, the time constant was estimated to be shorter in the case of the conjugated electrodes (i.e. 13.07 s) compared to those of the pure perovskite (i.e. 19.74 s) and pure rGO (i.e. 12.00 s) ones, indicating the shorter time required to attain the saturated charge conditions.

The performance stability of the electrodes is of crucial importance for energy storage applications. The conjugated electrodes developed in this work presented excellent stability behaviour, as the capacitance retention was preserved to 100%, even after 100 continuous Zn^{2+} intercalation/deintercalation cycles at 0.8 A g⁻¹ (Fig. 2f). This performance is in contrast to that of pure perovskite electrodes, where degradation was observed on the very first cycles, as mentioned above (Fig. 2c). This result stands as a proof-of-concept approach for the enhancement of capacitance resulting from the conjugation of perovskites and rGO flakes.

By comparing our results with other all-inorganic two-component graphene-related materials used in capacitors (including or not a complete capacitor cell) to date, it is clear that the metal halide perovskites–rGO electrodes due to the effective synergy of the EDLC and pseudocapacitance present the highest capacitance enhancement (Fig. 3a green arrow, Table S1†) and even if the amine-functionalized rGO was finally found, it was not the ideal choice because its EDLC capacitance was considerably low compared with other rGO electrode materials reported in the literature. As mentioned earlier in the text, the capacitance of the graphene-related materials in Zn-ion capacitors is correlated to the number of their defects, functional groups and impurities. Among the hybrid systems with the highest enhancement reported to date are the MnO₂–graphene[60,61] one and the MnSiO₃–GO hybrid composites.[47] It is important to notice here that the enhancement observed for our conjugates cannot be directly compared with the reported materials, as the electrolyte concentration utilized in these systems was practically double and based on monovalent ions (i.e. H⁺, K⁺, and Na⁺), making it easier for the ions to intercalate.

One can then realize that there is limited exploration of the investigation of all-inorganic two-component graphene-related
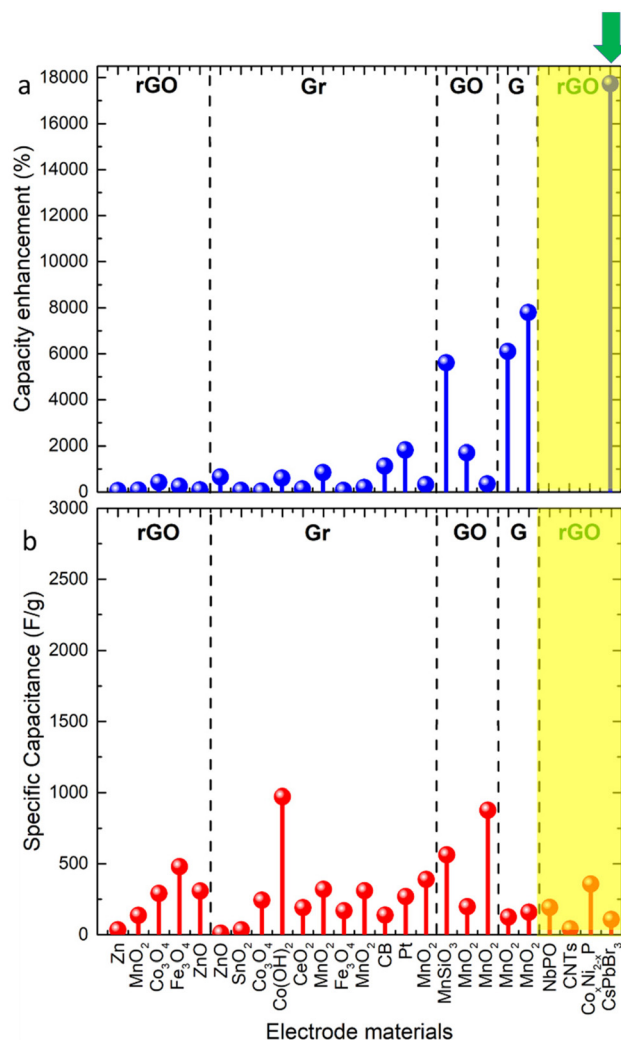

Fig. 3 Plots depicting the comparison of the capacitance enhancement compared to the values of single-2D material electrodes (a) and their corresponding specific capacitance in F g⁻¹ (b) of the CsPbBr₃ nanocrystal–rGO conjugates (indicated by the green arrow) with two-component hybrid systems reported to date. The Zn-ion capacitors are shown in the yellow box. The materials that are presented in this figure are: Zn/rGO,[62] MnO₂/rGO,[28] Co₃O₄/rGO,[33] Fe₃O₄/rGO,[36] ZnO/rGO,[34] ZnO/Gr,[63] SnO₂/Gr,[64] Co₃O₄/Gr,[32] Co(OH)₂/Gr,[65] CeO₂/Gr,[35] MnO₂/Gr,[66] Fe₃O₄/Gr,[67] MnO₂/Gr,[68] carbon black (CB)/Gr,[69] Pt/Gr,[70] MnO₂/Gr,[27] MnSiO₃/GO,[47] MnO₂/GO,[29] silver-doped MnO₂/GO,[30] MnO₂-G,[61] MnO₂/G,[60] NbPO/rGO,[41] carbon nanotubes (CNTs)/rGO,[42] and CoₓNi₂₋ₓP/rGO,[43] where rGO: reduced graphene oxide, Gr: graphene, GO: graphene oxide, and G: graphite.

materials as potential electrode components in Zn-ion capacitors, with only four studies reported so far (Fig. 3b). The capacitance enhancement in these hybrid systems cannot be quantified, as the capacitance of the pure graphene-related electrodes was not provided in these studies. The capacitance of metal halide perovskite–rGO conjugates is similar to that of the NbPO/rGO[41] ones, but lower than that of CoₓNi₂₋ₓP/rGO.[43] It is worth noting that our electrolyte concentration is four times lower than the one reported for the latter system. This

highlights the potential advantages of reduced cost, improved safety and enhanced environmental friendliness. It should be noted that the synthesis of the latter material required a prolonged and high temperature process at 180 °C for 16 hours. Nevertheless, compared to the carbon nanotubes/rGO composites,[42] the capacitance of the electrodes presented in this work is ~4 times higher even upon using four times lower electrolyte concentration.

3. Conclusions

Conjugated systems obtained by the attachment of metal halide perovskite nanocrystals onto rGO flakes through a laser-triggered method exhibited promising performance for Zn-ion capacitors. This is attributed to the synergy of the EDLC and pseudocapacitance originating from the different components involved. In particular, they showed a specific capacitance value of 106 F g^{-1} with an excellent stability remaining 100% after 100 continuous Zn^{2+} intercalation/deintercalation scans. The $CsPbBr_3$-rGO electrode exhibited the best stability and the highest specific capacitance compared with the single-component (i.e. rGO and $CsPbBr_3$ nanocrystals) electrodes. Overall, the room temperature laser-triggered technique selected for the conjugation of the two components provides a distinct avenue for the cost-effective and large-scale synthesis of precisely tailored perovskite–2D conjugates. This process allows one to bring together nanocrystals with various morphologies and chemical phases, along with multiple 2D materials, in the pursuit of discovering the most optimal combinations. Different 2D materials with large electrolyte contact areas and numerous energy storage active sites may serve as alternatives to the low capacitance NH_3-functionalized rGO for enhancing the capacitance of the conjugated systems. These efforts are aimed at further enhancing the electrochemical performance and long-term stability of the electrodes in Zn-ion capacitors. In addition, the data obtained in this work are a good basis for further study of perovskite–rGO conjugates through the control of the electrolyte concentration and pH value to enhance further the electrochemical performance. In this particular study, our emphasis was on exploring the utilization of metal halide nanocrystals conjugated with rGO flakes as electrodes for capacitors, establishing a foundational framework for subsequent investigations. Future work will assess the electrode performance in capacitor devices after further elevating their capacity.

Author contributions

Conceptualization: A. K., D. V. and K. B.; methodology: A. K., D. V. and K. B.; validation: N. L., S. D. and K. B.; formal analysis: A. K., D. V. and K. B; investigation: A. K., D. V. and K. B.; resources: E. S. and A. K.; data curation: A. K., D. V., and K. B.; writing – original draft preparation: A. K. and D. V.; writing – review and editing: A. K., D. V., K. B. and E. S.; visualization:

A. K. and D. V.; supervision: A. K., D. V, and E. S.; project administration: A. K. and E. S.; funding acquisition: E. S. and A. K. All authors have read and agreed to the published version of the manuscript.

Conflicts of interest

There are no conflicts to declare.

Acknowledgements

References

1 A. Kostopoulou, et al., Perovskite nanocrystals for energy conversion and storage, Nanophotonics, 2019, 8(10), 1607–1640, DOI: 10.1515/nanoph-2019-0119.

2 A. Kostopoulou, E. Kymakis and E. Stratakis, Perovskite nanostructures for photovoltaic and energy storage devices, J. Mater. Chem., 2018, A6(21), 9765–9798, DOI: 10.1039/C8TA01964A.

3 A. Kostopoulou, et al., All-inorganic lead halide perovskite nanohexagons for high performance air-stable lithium batteries, Nanoscale, 2019, 11(3), 882–889, DOI: 10.1039/C8NR10009H.

4 H. Yu, et al., CsPbCl3 and Mn:CsPbCl3 perovskite nanocubes/nanorods as a prospective cathode material for LIB application, J. Mater. Sci.: Mater. Electron., 2023, 34(21), 1582, DOI: 10.1007/s10854-023-10998-3.

5 Q. Wang, et al., Morphological and chemical tuning of lead halide perovskite mesocrystals as long-life anode materials in lithium-ion batteries, CrystEngComm, 2019, 21(6), 1048–1059, DOI: 10.1039/C8CE01779D.

6 H.-R. Xia, W.-T. Sun and L.-M. Peng, Hydrothermal synthesis of organometal halide perovskites for Li-ion batteries, Chem. Commun., 2015, 51(72), 13787–13790, DOI: 10.1039/C5CC05053G.

7 A. Kostopoulou, et al., Highly stable metal halide perovskite microcube anodes for lithium-air batteries, J. Power Sources Adv., 2020, 3, 100015, DOI: 10.1016/j.powera.2020.100015.

8 Q. Wang, et al., NH3-induced morphological evolution of organohalide perovskites from three-dimensional micro-cubes to one-dimensional nanorod aggregates and their electrochemical performance, Mater. Today Chem., 2019, **12**, 343–352, DOI: **10.1016/j.mtchem.2019.03.007**.

9 M. Tathavadekar, et al., Low-dimensional hybrid perovskites as high performance anodes for alkali-ion batteries, J. Mater. Chem. A, 2017, **5**(35), 18634–18642, DOI: **10.1039/C7TA04529H**.

10 P. Pal and A. Ghosh, Three-Dimensional $\mathrm{Cs}\mathrm{Pb}\mathrm{Cl}_{3}$ Perovskite Anode for Quasi-Solid-State Li-Ion and Dual-Ion Batteries: Mechanism of Li^{+} Conversion Process in Perovskite, Phys. Rev. Appl., 2020, **14**(6), 064010, DOI: **10.1103/PhysRevApplied.14.064010**.

11 P. Pandey, et al., Realization of High Capacity and Cycling Stability in Pb-Free A2CuBr4 (A=CH₃NH3/Cs, 2 D/3 D) Perovskite-Based Li-Ion Battery Anodes, ChemSusChem, 2019, **12**(16), 3742–3746, DOI: **10.1002/cssc.201900959**.

12 S. Zhou, et al., Thin Film Electrochemical Capacitors Based on Organolead Triiodide Perovskite, Adv. Electron. Mater., 2016, **2**(7), 1600114, DOI: **10.1002/aelm.201600114**.

13 I. Popoola, et al., Fabrication of organometallic halide perovskite electrochemical supercapacitors utilizing quasi-solid-state electrolytes for energy storage devices, Electrochim. Acta, 2019, **332**, 135536, DOI: **10.1016/j.electacta.2019.135536**.

14 T. Li, et al., Thiourea Bismuth Iodide: Crystal Structure, Characterization and High Performance as an Electrode Material for Supercapacitors, Batteries Supercaps, 2019, **2**(6), 568–575, DOI: **10.1002/batt.201900005**.

15 J. K. Pious, et al., Zero-Dimensional Methylammonium Bismuth Iodide-Based Lead-Free Perovskite Capacitor, ACS Omega, 2017, **2**(9), 5798–5802, DOI: **10.1021/acsomega.7b00973**.

16 Y. Qian, et al., Emerging perovskite materials for supercapacitors: Structure, synthesis, modification, advanced characterization, theoretical calculation and electrochemical performance, J. Energy Chem., 2024, **89**, 41–70, DOI: **10.1016/j.jechem.2023.10.028**.

17 S. Tudu, et al., Fabrication of CH₃NH3SnCl3 perovskite nanocrystal-based electrode for supercapacitor devices application, J. Alloys Compd., 2024, **971**, 172554, DOI: **10.1016/j.jallcom.2023.172554**.

18 M. S. Ali, et al., Ultrahigh energy density solid state supercapacitor based on metal halide perovskite nanocrystal electrodes: Real-life applications, J. Energy Storage, 2023, **65**, 107215, DOI: **10.1016/j.est.2023.107215**.

19 S. Thakur, et al., All-inorganic CsPbBr₃ perovskite as potential electrode material for symmetric supercapacitor, Solid State Sci., 2021, **122**, 106769, DOI: **10.1016/j.solidstatesciences.2021.106769**.

20 M. Pumera, Graphene-based nanomaterials for energy storage, Energy Environ. Sci., 2011, **4**(3), 668–674, DOI: **10.1039/C0EE00295J**.

21 M. I. A. Abdel Maksoud, et al., Advanced materials and technologies for supercapacitors used in energy conversion and storage: a review, Environ. Chem. Lett., 2021, **19**(1), 375–439, DOI: **10.1007/s10311-020-01075-w**.

22 R. Rojaee and R. Shahbazian-Yassar, Two-Dimensional Materials to Address the Lithium Battery Challenges, ACS Nano, 2020, **14**(3), 2628–2658, DOI: **10.1021/acsnano.9b08396**.

23 Y. Nishi, Lithium ion secondary batteries; past 10 years and the future, J. Power Sources, 2001, **100**(1), 101–106, DOI: **10.1016/S0378-7753(01)00887-4**.

24 X. Cai, et al., Graphene and graphene-based composites as Li-ion battery electrode materials and their application in full cells, J. Mater. Chem. A, 2017, **5**(30), 15423–15446, DOI: **10.1039/C7TA04354F**.

25 G. Huang, B. Cai, C. Zhan, P. Sun and G. Huang, Two-dimensional Material as Anode for Lithium Ion Batteries: Recent Progress, Int. J. Electrochem. Sci., 2020, 5416–5429, DOI: **10.20964/2020.06.72**.

26 X. Zhu, Recent advances of transition metal oxides and chalcogenides in pseudo-capacitors and hybrid capacitors: A review of structures, synthetic strategies, and mechanism studies, J.Energy Storage, 2022, **49**, 104148, DOI: **10.1016/j.est.2022.104148**.

27 B. G. Choi, et al., 3D Macroporous Graphene Frameworks for Supercapacitors with High Energy and Power Densities, ACS Publications, 2012, DOI: **10.1021/nn3003345**, (accessed 15 February 2023).

28 Z. Li, et al., Synthesis of hydrothermally reduced graphene/MnO₂ composites and their electrochemical properties as supercapacitors, J. Power Sources, 2011, **196**(19), 8160–8165, DOI: **10.1016/j.jpowsour.2011.05.036**.

29 S. Chen, et al., Graphene Oxide−MnO₂ Nanocomposites for Supercapacitors, ACS Nano, 2010, **4**(5), 2822–2830, DOI: **10.1021/nn901311t**.

30 V. J. Mane, et al., Enhanced specific energy of silver-doped MnO₂/graphene oxide electrodes as facile fabrication symmetric supercapacitor device, Mater. Today Chem., 2021, **20**, 100473, DOI: **10.1016/j.mtchem.2021.100473**.

31 B. Gangopadhyay, et al., Thermal Effects on Electrochemical Performance of Copper Oxide Nanoparticles Decorated Amine-Functionalized Graphene Oxide for Ultrahigh Energy Density Supercapacitor with Real-Life Application, J. Phys. Chem. C, 2023, **127**(45), 21940–21953, DOI: **10.1021/acs.jpcc.3c03190**.

32 J. Yan, et al., Rapid microwave-assisted synthesis of graphene nanosheet/Co3O4 composite for supercapacitors, Electrochim. Acta, 2010, **55**(23), 6973–6978, DOI: **10.1016/j.electacta.2010.06.081**.

33 H.-W. Wang, et al., Preparation of reduced graphene oxide/cobalt oxide composites and their enhanced capacitive behaviors by homogeneous incorporation of reduced graphene oxide sheets in cobalt oxide matrix, Mater. Chem. Phys., 2011, **130**(1), 672–679, DOI: **10.1016/j.matchemphys.2011.07.043**.

34 Y.-L. Chen, *et al.*, Zinc Oxide/Reduced Graphene Oxide Composites and Electrochemical Capacitance Enhanced by Homogeneous Incorporation of Reduced Graphene Oxide Sheets in Zinc Oxide Matrix, *J. Phys. Chem. C*, 2011, **115**(5), 2563–2571, DOI: **10.1021/jp109597n**.

35 Y. Wang, *et al.*, CeO_2 nanoparticles/graphene nanocomposite-based high performance supercapacitor, *Dalton Trans.*, 2011, **40**(24), 6388–6391, DOI: **10.1039/C1DT10397K**.

36 W. Shi, *et al.*, Achieving high specific charge capacitances in Fe3O4/reduced graphene oxide nanocomposites, *J. Mater. Chem.*, 2011, **21**(10), 3422–3427, DOI: **10.1039/C0JM03175E**.

37 Y. Li, *et al.*, Recent progress and perspective of multifunctional integrated zinc-ion supercapacitors, *Energy Mater.*, 2022, **2**(3), 200018, DOI: **10.20517/energymater.2022.15**.

38 D. Zhang, *et al.*, A new type of zinc ion hybrid supercapacitor based on 2D materials, *Nanoscale*, 2021, **13**(25), 11004–11016, DOI: **10.1039/D1NR03215A**.

39 A. Ambrosi, *et al.*, Electrochemistry of Graphene and Related Materials, *Chem. Rev.*, 2014, **114**(14), 7150–7188, DOI: **10.1021/cr500023c**.

40 H. Xu, *et al.*, Revisiting Charge Storage Mechanism of Reduced Graphene Oxide in Zinc Ion Hybrid Capacitor beyond the Contribution of Oxygen-Containing Groups, *Adv. Funct. Mater.*, 2022, **32**(16), 2111131, DOI: **10.1002/adfm.202111131**.

41 S. J. Patil, *et al.*, Ultra-stable flexible Zn-ion capacitor with pseudocapacitive 2D layered niobium oxyphosphides, *Energy Storage Mater.*, 2022, **45**, 1040–1051, DOI: **10.1016/j.ensm.2021.10.040**.

42 T. Ni, *et al.*, Highly Flexible and Self-Healable Zinc-Ion Hybrid Supercapacitors Based on MWCNTs-RGO Fibers, *Adv. Mater. Technol.*, 2020, **5**(9), 2000268, DOI: **10.1002/admt.202000268**.

43 D. Guo, *et al.*, Design and Synthesis of Zinc-Activated CoxNi2−xP/Graphene Anode for High-Performance Zinc Ion Storage Device, *ChemSusChem*, 2021, **14**(10), 2205–2215, DOI: **10.1002/cssc.202100285**.

44 Y.-F. Xu, *et al.*, A $CsPbBr_3$ Perovskite Quantum Dot/ Graphene Oxide Composite for Photocatalytic CO2 Reduction, *J. Am. Chem. Soc.*, 2017, **139**(16), 5660–5663, DOI: **10.1021/jacs.7b00489**.

45 X. Tang, *et al.*, $CsPbBr_3$/Reduced Graphene Oxide nanocomposites and their enhanced photoelectric detection application, *Sens. Actuators, B*, 2017, **245**, 435–440, DOI: **10.1016/j.snb.2017.01.168**.

46 Q. Wang, *et al.*, Graphene oxide wrapped CH3NH3PbBr3 perovskite quantum dots hybrid for photoelectrochemical CO2 reduction in organic solvents, *Appl. Surf. Sci.*, 2019, **465**, 607–613, DOI: **10.1016/j.apsusc.2018.09.215**.

47 Y. Cheng, *et al.*, Synthesis of amorphous MnSiO3/graphene oxide with excellent electrochemical performance as supercapacitor electrode, *Colloids Surf., A*, 2019, **562**, 93–100, DOI: **10.1016/j.colsurfa.2018.11.011**.

48 J. Xu, *et al.*, Recent Research of NiCo2O4/Carbon Composites for Supercapacitors, *Surfaces*, 2022, **5**(3), 334–349, DOI: **10.3390/surfaces5030025**.

49 T. Wang, *et al.*, MnO Nanoparticle@Mesoporous Carbon Composites Grown on Conducting Substrates Featuring High-performance Lithium-ion Battery, Supercapacitor and Sensor, *Sci. Rep.*, 2013, **3**(1), 2693, DOI: **10.1038/srep02693**.

50 A. Azhar, *et al.*, Nanoporous Iron Oxide/Carbon Composites through *In situ* Deposition of Prussian Blue Nanoparticles on Graphene Oxide Nanosheets and Subsequent Thermal Treatment for Supercapacitor Applications, *Nanomaterials*, 2019, **9**(5), 776, DOI: **10.3390/nano9050776**.

51 T. Li and H. Liu, A simple synthesis method of nanocrystals CeO_2 modified rGO composites as electrode materials for supercapacitors with long time cycling stability, *Powder Technol.*, 2018, **327**, 275–281, DOI: **10.1016/j.powtec.2017.12.073**.

52 A. Ganiyat Olatoye, *et al.*, Synthesis of γ-MnS/nanoporous carbon/reduced graphene oxide composites for high-performance supercapacitor, *Carbon Resour. Convers.*, 2022, **5**(3), 222–230, DOI: **10.1016/j.crcon.2022.06.002**.

53 X. Li, *et al.*, CsPbX3 Quantum Dots for Lighting and Displays: Room-Temperature Synthesis, Photoluminescence Superiorities, Underlying Origins and White Light-Emitting Diodes, *Adv. Funct. Mater.*, 2016, **26**(15), 2435–2445, DOI: **10.1002/adfm.201600109**.

54 A. Kostopoulou, *et al.*, Laser-Assisted Fabrication for Metal Halide Perovskite-2D Nanoconjugates: Control on the Nanocrystal Density and Morphology, *Nanomaterials*, 2020, **10**(4), 747, DOI: **10.3390/nano10040747**.

55 F. He, *et al.*, Hydrothermal synthesis of Ni-based metal organic frameworks/graphene oxide composites as supercapacitor electrode materials, *J. Mater. Res.*, 2020, **35**(11), 1439–1450, DOI: **10.1557/jmr.2020.93**.

56 C. Zhu, *et al.*, Binder-free stainless steel@Mn3O4 nanoflower composite: a high-activity aqueous zinc-ion battery cathode with high-capacity and long-cycle-life, *J. Mater. Chem.*, 2018, **A6**(20), 9677–9683, DOI: **10.1039/C8TA01198B**.

57 J.-G. Wang, *et al.*, Onion-like nanospheres organized by carbon encapsulated few-layer MoS2 nanosheets with enhanced lithium storage performance, *J. Power Sources*, 2019, **413**, 327–333, DOI: **10.1016/j.jpowsour.2018.12.055**.

58 Y. Wang, *et al.*, Flexible supercapacitor with high energy density prepared by GO-induced porous coral-like polypyrrole (PPy)/PET non-woven fabrics, *J. Mater. Sci.*, 2018, **53**(11), 8409–8419, DOI: **10.1007/s10853-018-2131-9**.

59 Y. Liu, *et al.*, Layered-MnO2 Nanosheet Grown on Nitrogen-Doped Graphene Template as a Composite Cathode for Flexible Solid-State Asymmetric Supercapacitor, *ACS Appl. Mater. Interfaces*, 2016, **8**(8), 5251–5260, DOI: **10.1021/acsami.5b10649**.

60 J. Yan, *et al.*, Preparation and electrochemical characteristics of manganese dioxide/graphite nanoplatelet composites, *Mater. Sci. Eng. B*, 2008, **151**(2), 174–178, DOI: **10.1016/j.mseb.2008.05.018**.

61 C. Wan, K. Azumi and H. Konno, Hydrated Mn(IV) oxide-exfoliated graphite composites for electrochemical capacitor, *Electrochim. Acta*, 2007, **52**(9), 3061–3066, DOI: **10.1016/j.electacta.2006.09.039**.

62 M. Ates, S. Caliskan and E. Özten, Supercapacitor study of reduced graphene oxide/Zn nanoparticle/polycarbazole electrode active materials and equivalent circuit models, *J. Solid State Electrochem.*, 2018, **22**(10), 3261–3271, DOI: **10.1007/s10008-018-4039-3**.

63 Y. Zhang, *et al.*, Capacitive behavior of graphene–ZnO composite film for supercapacitors, *J. Electroanal. Chem.*, 2009, **634**(1), 68–71, DOI: **10.1016/j.jelechem.2009.07.010**.

64 F. Li, *et al.*, One-step synthesis of graphene/SnO2 nanocomposites and its application in electrochemical supercapacitors, *Nanotechnology*, 2009, **20**(45), 455602, DOI: **10.1088/0957-4484/20/45/455602**.

65 S. Chen, J. Zhu and X. Wang, One-Step Synthesis of Graphene–Cobalt Hydroxide Nanocomposites and Their Electrochemical Properties, *J. Phys. Chem. C*, 2010, **114**(27), 11829–11834, DOI: **10.1021/jp1048474**.

66 M. N. Dang, *et al.*, One-pot synthesis of manganese oxide/graphene composites via a plasma-enhanced electrochemical exfoliation process for supercapacitors, *Nanotechnology*, 2020, **31**(34), 345401, DOI: **10.1088/1361-6528/ab8fe5**.

67 Q. Ke, *et al.*, Intercalating graphene with clusters of Fe3O4 nanocrystals for electrochemical supercapacitors, *Mater. Res. Express*, 2014, **1**(2), 025015, DOI: **10.1088/2053-1591/1/2/025015**.

68 J. Yan, *et al.*, Fast and reversible surface redox reaction of graphene–MnO$_2$ composites as supercapacitor electrodes, *Carbon*, 2010, **48**(13), 3825–3833, DOI: **10.1016/j.carbon.2010.06.047**.

69 G. Wang, *et al.*, Flexible Pillared Graphene-Paper Electrodes for High-Performance Electrochemical Supercapacitors, *Small*, 2012, **8**(3), 452–459, DOI: **10.1002/smll.201101719**.

70 Y. Si and E. T. Samulski, Exfoliated Graphene Separated by Platinum Nanoparticles, *Chem. Mater.*, 2008, **20**(21), 6792–6797, DOI: **10.1021/cm801356a**.